Hindawi
Advances in Civil Engineering
Volume 2022, Article ID 7401917, 14 pages
https://doi.org/10.1155/2022/7401917

Research Article

Analysis of Influencing Parameters of the Improved Model for Rainfall Infiltration in Unsaturated Tailings Soil

Qingchao Yang,[1,2] Zhe Hao,[3] Wenjing Cheng,[2] Shengyou Lei,[1] Da Teng,[4,5,6] Ying Zhang,[4,5,6] Xiaoming Wang,[4,5,6] and Qian Zhang[4,5,6]

[1]*School of Highway, Chang'an University, Xi'an 710064, China*
[2]*School of Highway and Architecture, Shandong Transport Vocational College, Weifang 261206, China*
[3]*College of Environmental Sciences, Liaoning University, Shenyang 110036, China*
[4]*Liaoning Nonferrous Geological Exploration and Research Institute Co, Shenyang 110013, China*
[5]*Liaoning Provincial Key Laboratory of Mine Environment Geotechnical Engineering, Shenyang 110013, China*
[6]*Technology Innovation Center for Old Mine Geological Disaster Prevention and Ecological Restoration, Ministry of Natural Resources, Shenyang, 110013, China*

Correspondence should be addressed to Zhe Hao; 2017021004@chd.edu.cn

Received 30 March 2022; Revised 25 May 2022; Accepted 16 June 2022; Published 16 July 2022

Academic Editor: Jian Ji

The rainfall infiltration analysis method is an important method for slope stability forecast and prevention. Slope angle and unsaturated soil layers are not shown in the conventional Green-Ampt (GA) infiltration model. In this paper, based on the GA model of rainfall infiltration in tailings slopes, two aspects of slope angle and the proportion of the transition layer of the wet layer are modified. The rainfall infiltration test of unsaturated tailing soil was conducted using a self-developed large-size tailing slope model test device. The results of GA model, improved GA model, and Richards' equation calculation model are compared. The results show that the difference between the three models is small in the free infiltration stage, but the infiltration rate is lower than that of the GA model. With the gradual increase of rainfall time into the ponding infiltration stage, the expansion depth and infiltration rate of the wetting front of the improved GA model and Richards' equation are greater than those of the GA model. The difference between the GA model and the improved GA model and Richards' equation for the extended depth of wetting front increases with the increase of rainfall duration, while the difference of infiltration rate changes in the opposite trend. The results of the improved GA model and Richards' equation to calculate the expansion depth and infiltration rate of wetting fronts are consistent, and the difference basically tends to stabilize with the increase of rainfall ephemeris. The results of the improved GA model are closer to the measured data, which can provide a reference for analyzing the rainfall infiltration pattern of open pit tailing dams and slope stability research. On the basis of the improved GA model, the influence of slope angle, rain intensity, initial water content, and saturation infiltration coefficient on rainfall infiltration was analyzed, and the analysis of parameter sensitivity indexes showed that slope inclination and initial water content had a greater influence on the model.

1. Introduction

Tailings storage facility is an important integrated structure for storing tailings [1] and a major source of danger with high potential energy [2]. Due to a large number of unsaturated tailings with loose structures [2, 3], it is easy to cause dam failures under continuous rainfall [4, 5]. Therefore, studying rainfall infiltration law of unsaturated tailings soil and establishing an accurate prediction model is of great theoretical significance and practical value for improving the safe and stable operation of the tailings pond under the condition of rainfall [6] and tailings pond accident prediction [3, 7, 8]. For rainfall infiltration on slopes, many scholars have used simplified rainfall infiltration models to predict the infiltration characteristics of slopes [9]. Green-Ampt (GA) infiltration model [10, 11] is widely used in the study of rainfall infiltration problems on slopes by intuitively solving the advancement of wetting fronts [12]. Jahanshir and

Manouchehr [13] and Deng and Zhu [14] further extended the applicability of the GA model by considering vertically stratified soil parameters and effective suction values. Yao et al. [15] explored the effect of the extended model on the shallow stability of slopes under rainfall conditions. Richa et al. [16] found an analytical expression for the effective saturated hydraulic conductivity and analyzed the infiltration rate of unsaturated soils and the evolutionary characteristics of soil surface moisture under rainfall conditions. Wang et al. [17] established a numerical model of flow-solid coupling on the slope of foundation pits with soil-rock composite strata to analyze the change law of hydraulic coupling caused by rainfall. Guo et al. [18] analyzed the effect of inhomogeneous initial water content on the improved GA model in conjunction with the field monitoring results. Sanghyun et al. [19] investigated a simplified model applying the GA method to a two-layer soil body. Fernández et al. [20] proposed a modified GA model of rainfall and runoff to estimate infiltration rates and cumulative infiltration. Sung [21] and Pan et al. [22] modified the GA model by considering an initial inhomogeneous water content distribution and a constant rainfall intensity. Wen et al. [23] and Peng et al. [24] discussed the stratification characteristics of the GA infiltration model under ponding conditions, but none of them discussed the scaling of the actual stratification thickness and the slope environment under the stratification assumption.

At present, the calculation of rainfall infiltration depth has a certain theoretical basis, but the GA model applied to unsaturated tailings soil has more deficiencies, and the improvement of the accuracy of the model also needs further exploration. Therefore, the slope angle of the tailings slope and the ratio of the transition layer to the wetted layer on the slope were modified on the basis of the GA model. The effects of slope angle, rain intensity, initial water content, and saturation infiltration coefficient on the depth of rainfall infiltration were analyzed according to the modified model, and the sensitivity of relevant parameters of the model was analyzed to provide a reference for studying the tailings dams' stability under the action of rainfall.

2. Study Method

2.1. Classical GA Infiltration Model. During continuous rainfall, the rainfall infiltration process of slopes is influenced by the slope water content and slope volume water [25] and the traditional GA model was initially used to analyze the saturated infiltration of slopes under rainfall conditions. The schematic diagram of GA infiltration model is shown in Figure 1, according to [26] with some modifications. θ_s is the saturated water content of unsaturated slope soils; θ_i is the initial water content of unsaturated slope soil; $h_0$is the depth of water accumulation on the horizontal surface of the unsaturated soil; $h_d$is the depth of the wetting front in the vertical direction.

The soil is assumed as a homogeneous mass in the model. The wetting front formed by the rainfall infiltration serves as the partition interface between the wetted layer's saturated water content and the unwetted layer's initial water content.

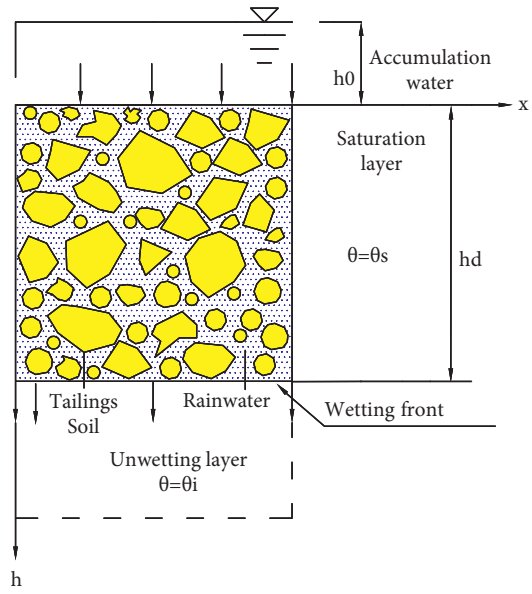

Figure 1: The schematic diagram of GA infiltration model.

The matrix suction of the soil below the wetting front is considered to be constant.

According to the characteristics of rainfall infiltration, it is divided into two stages [19, 26–28]: Stage I is defined as the free infiltration stage, which is characterized by the soil infiltration coefficient greater than the rainfall intensity, so the soil rainfall infiltration boundary is controlled by the rainfall intensity to reflect. Stage II is defined as the ponding infiltration stage, which is characterized by the rainfall intensity greater than the soil infiltration coefficient, so the soil rainfall infiltration boundary is controlled by the soil infiltration capacity to reflect.

It is assumed that t_p is the time elapsed in the transition from stage I to stage II. Z_{fp} is the depth of the wetting front at the moment of t_p.

The relationship between the depth of the wetting front and the infiltration time in the free infiltration stage I of rainfall is shown in the following equation:

$$h_d = \frac{q}{\theta_s - \theta_i} t, \quad 0 \le t \le t_p, \tag{1}$$

where q is the magnitude of rainfall intensity; $t_p = (\theta_s - \theta_i)S_f/q(q/k_s - 1)$; k_s is the saturated permeability coefficient of unsaturated slope soils; and S_f is the substrate potential head of the unwetted layer relative to the saturated layer. The substrate potential head is taken as half of the water potential corresponding to the inlet pressure value of the soil [17, 20, 29].

When the infiltration surface is inclined, the accumulation of water is difficult to happen. The effect of water accumulation h_0 is negligible. The depth of the wetting front as a function of rainfall time is given in the following equation:

$$t - t_p = \frac{\theta_s - \theta_i}{k_s}\left(z_f - z_p - s_f In\frac{z_s + s_f}{z_{fp} + s_f}\right), \quad t > t_p, \tag{2}$$

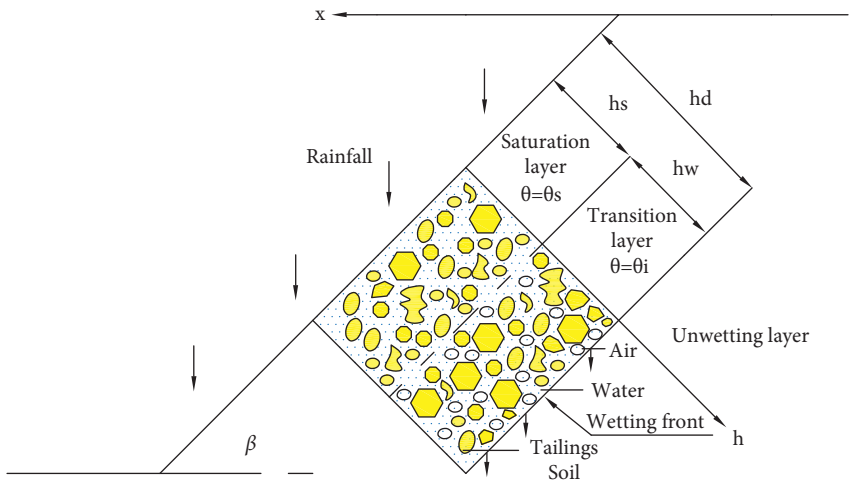

Figure 2: The schematic diagram of improved GA infiltration model.

where $Z_{fp} = S_f/(q/k_s - 1)$.

Equations (1) and (2) are the control equations of the traditional GA infiltration model, which are simple in structure and convenient to solve. However, the influence of slope angle and unsaturated zone on rainfall infiltration was not considered in the equations, which deviates greatly from the actual situation.

2.2. Improved Infiltration Model. According to seepage characteristics of unsaturated tailings soil air in the pore space prevents the wetted zone from being fully saturated [3, 30]. Based on the assumption of saturated-unsaturated stratification of rainfall infiltration in tailings slope, the schematic diagram of improved GA infiltration model is shown in Figure 2.

The basic assumptions of the improved GA infiltration model are as follows:

(1) Following the GA model, a well-defined wetting front exists, and the water content of the soil before the wetting front is the initial water content.

(2) The tailing soil slope is divided into wetted and unwetted layers, and the infiltration process adopts the layering assumption, and the wetted layer is divided into the saturated and transition layers.

(3) To improve the accuracy of calculating the moisture content of the wetted layer during rainfall, a 1/4 elliptical curve representation is used.

Assumptions (1) and (2) have been used extensively in the published literature [23, 24, 28, 31–34] which have been shown to be reasonable, where the intersection of the transition region with the natural region is referred to as the wetted peak surface.

The experimental results of hypothesis (3) in the published literature [23, 24, 33, 34] have verified the reasonableness of hypothesis (3).

Saturation layer is as follows:

$$\theta(h) = \theta_s, 0 \le h \le h_p. \tag{3}$$

Transition layer is as follows:

$$\theta(h) = \theta_d + (\theta_s - \theta_d)\sqrt{1 - [(h - h_s)/h_w]^2} hs \le h \le h_d. \tag{4}$$

Unwetted layer is as follows:

$$\theta(h) = \theta_d, \quad h \ge h_d. \tag{5}$$

In published literatures [15, 23, 24, 33, 34], experimental results have verified the validity and correctness of the equations for the volumetric water content (3)–(5) of the soil profile.

$$h_s = h_d - h_w = (1 - \lambda)h_d, \tag{6}$$

where h_s is the saturation layer depth; h_w is the transition layer depth; h_d is the unwetted layer depth; and $\lambda = h_w/h_d$.

Cumulative measurement of rainwater infiltration into unsaturated tailings soil is as follows:

$$I = \int_0^h [\theta(h) - \theta_d]dh. \tag{7}$$

Saturation layer is as follows:

$$I_s = (\theta_s - \theta_d)h_s. \tag{8}$$

Transition layer is as follows:

$$I_w = \frac{\pi}{4}(\theta_s - \theta_d)h_w,$$
$$I = I_s + I_w = (\theta_s - \theta_d)h_s + \frac{\pi}{4}(\theta_s - \theta_d)h_w. \tag{9}$$

It is assumed that, in the initial stage of slope rainfall, rainfall can completely penetrate into tailings soil.

$$i = q\cos\beta, \tag{10}$$

where β is the slope angle and i is the infiltration rate.

According to Darcy's law, the infiltration rate during the infiltration stage of ponded water can be expressed as follows:

$$i = k_s\left(\frac{h_s\cos\beta + S_f' + h_0}{h_s}\right), \tag{11}$$

where S_f' is the matrix potential head applied to the saturated layer by the transition layer.

It is obtained according to the studies of Peng et al. [24] and Zhu and Duan [27].

$$S_f' = \frac{\overline{k}}{k_s} S_f = \frac{1 - (k_i/k_s)}{\ln (k_s/k_i)} S_f, \tag{12}$$

where $\overline{k}$ is the equivalent value of permeability coefficient of transition layer soil and k_i is the equivalent values of permeability coefficients for unsaturated soils in the unwetted layer.

It is assumed that t_p is the time elapsed in transition from stage I to stage II. The wetting front depth and infiltration rate of unsaturated slope vertical slope at the moment of t_p are Z_p and i_p, respectively.

$$\begin{aligned} q\cos\beta\, dt &= \frac{[4 + (\pi - 4)\lambda]}{4} (\theta_s - \theta_i) dh_d, \\ q\cos\beta = i_p &= k_s \frac{(1-\lambda)h_d \cos\beta + S_f' + h_0}{(1-\lambda)h_d}. \end{aligned} \tag{13}$$

When the infiltration surface is inclined, water accumulation can hardly occur. The accumulation of water h_0 can be ignored. It can be simplified to the following equation:

$$h_d = \frac{4q\cos\beta}{[4 + (\pi - 4)\lambda](\theta_s - \theta_i)} t \quad 0 \le t \le t_p. \tag{14}$$

The depth of rainfall infiltration when ponding infiltration first begins to occur is h_p.

$$h_p = \frac{S_f'}{(1-\lambda)\cos\beta((q/k_s) - 1)}. \tag{15}$$

The time required for infiltration of accumulated water to occur is t_p.

$$t_p = \frac{[4 + (\pi - 4)\lambda](\theta_s - \theta_i) S_f'}{4(1-\lambda) q \cos^2\beta((q/k_s) - 1)}. \tag{16}$$

After entering stage II,

$$k_s \frac{\lambda h_d \cos\beta + S_f' + h_0}{\lambda h_d} \mathrm{d}t = \frac{[4 + (\pi - 4)\lambda]}{4} (\theta_s - \theta_i) \mathrm{d}h_d, \quad t > t_p, \tag{17}$$

note the boundary conditions $t = t_p$ and $h_d = h_p$, while ignoring h, the differential equation is solved.

$$t - t_p = \frac{[4 + (\pi - 4)\lambda]}{4k_s \cos\beta} (\theta_s - \theta_i) \left(h_d - h_p - \frac{S_f'}{\lambda \cos\beta} \mathrm{In} \frac{S_f' + \lambda \cos\beta h_d}{S_f' + \lambda \cos\beta h_p} \right), \quad t > t_p, \tag{18}$$

In summary, the effects of slope angle and unsaturated zone layer conditions were considered in equations (14) and (18) for the rainfall infiltration model.

3. Experimental Validation of Rainfall Model for Tailings Slope

3.1. Experimental Model. The self-developed test device for tailings rainfall infiltration model includes a model box and rainfall device, as shown in Figure 3. The test model's length, width, and height are 7 m, 1.2 m, and 1.8 m, respectively, forming a five-sided closed rectangular body. One side is a 7 m long transparent plexiglass board with the thickness of 1 cm, the other three sides are made of cement brick, the top is open, the bottom is evenly paved with a 10 cm thick gravel layer, and the permeable geotextile is laid above to form the tailing slope drainage channel. The rainfall system of rainfall infiltration model test device is mainly composed of automatic water make-up ball valve water tank, automatic frequency conversion constant pressure water pump, plastic water pipe, stainless steel vacuum water pressure gauge, high-precision electronic turbine flowmeter, rainfall device, electric elevator, and water retaining curtain. Rainfall device uses 20 mm diameter PVC pipe with 50 mm hole spacing and 1 mm diameter of the hole. The elbow is connected by right-angle tees. The rainfall intensity is controlled by a flow meter and copper valve, and the range of rainfall intensity is 10~280 mm/h to follow the test setting requirements. The elevator is adopted in the model system to adjust the height of the rainfall device, and the maximum height above the ground can reach 4.5 m. The water retaining curtain is set around the rainfall device to prevent the rainfall splashing.

3.2. Model Filling. To better match the actual operating conditions of tailings dams, tailings sands were excavated using the profile method to locate within 2 m of the burial depth in front of a tailings pond site [25]. The slope in the tailing model tank is 4.48 m long, 1.2 mm wide, 1.2 m high. The layered compaction method is used to establish the model of dam construction, as shown in Figure 4.

3.3. Monitoring Equipment and Programs. In the rainfall model, the nozzles of the simulated rainfall device were evenly distributed at a 4.5 m vertical distance of rainfall device from the horizontal surface of the bottom of the slope, and the rainfall intensity was set at 20 mm/h for this test. The rainfall intensity test was completed before the test. Firstly, the rain cloth was used to cover the test model. After the rainfall intensity reached 20 mm/h and the monitoring values were stable, the rain cloth was removed to start the formal experiment, and the rainfall lasted for 5 hours. Because the groundwater depth of the large- and medium-sized tailings pond slope is more than 4 m in practical, far lower

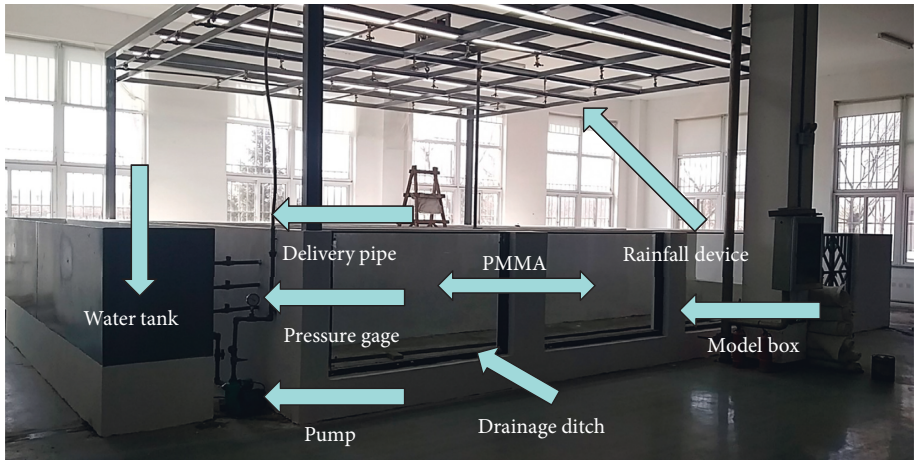

Figure 3: Rainfall test model for tailings slope.

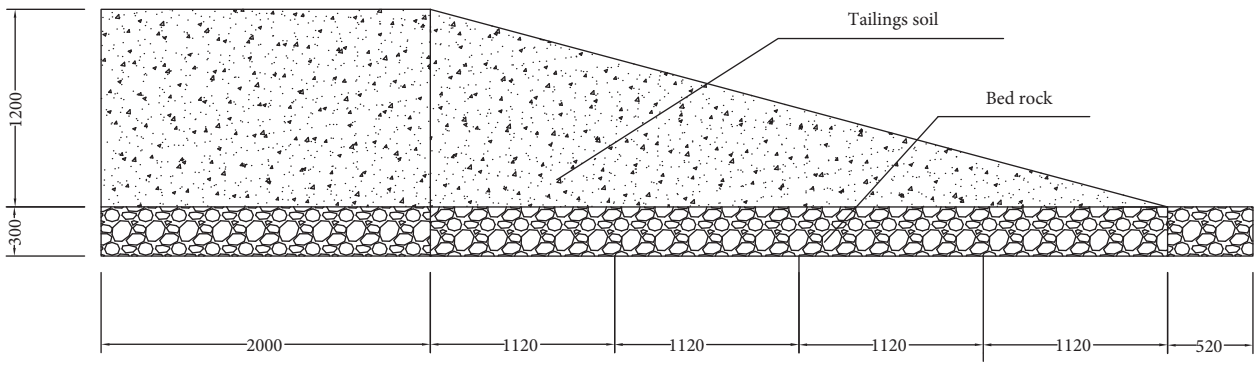

Figure 4: Schematic diagram of model filling (distance measured in mm).

than the rainfall infiltration area, this paper ignores the influence of groundwater on slope infiltration. The water content and pore water pressure sensors were arranged at the toe, middle, and shoulder of the tailings dam, and the vertical distance from the slope surface was 10, 20, and 30 cm, respectively, represented by *T* and *U*. In order to avoid mutual interference between *T* and *U* sensors in the same layer, they were arranged with a horizontal interval of 60 cm. The sensor number and position are represented by *Txy* and *Uxy*, where *x* indicates the sensor position number and *y* indicates the sensor's vertical depth from the slope.

For example, T110 is a soil volumetric moisture sensor with a vertical depth of 10 cm in the middle of the slope. The sensor in the model is linked with the data acquisition instrument, and the data is automatically recorded every 1 min. The tensiometer is 10 cm away from the boundary of the model and 56 cm away from the toe and shoulder of the slope, and the horizontal distance between each tensiometer is 112 cm. S represents tensiometer, the meanings of *x* and *y* are the same as mentioned above, and the data is recorded every 10 min. The specific burial location of the monitoring equipment is shown in Figure 5.

4. Model Validation and Analysis

4.1. Model Validation. The basic physical and mechanical parameters of the tailing soil at a depth of 5 cm from the slope surface in the model trough were precisely measured, as shown in Table 1. The soil and water characteristic curve and permeability coefficient curve of the tailing soil are shown in Figure 6 and Figure 7.

The positions T110, T120, and T130 were selected, and the moisture sensor data were collated when the wetting front arrived at different depths; the variation curves of volumetric moisture content with rainfall duration at different depths are shown in Figure 8.

Figure 8 shows that once the moisture sensor in the model soil responds, the volumetric water content gradually increases from the initial 12% to 30% in a saturated state with the increase of rainfall duration. It indicates that the layers transit from the initial state to the saturated state with the moisture content in the soil at each depth under the rainfall conditions.

Figure 9 shows the variation of pore water pressure and wetting front depth with different rainfall durations. The curves U120, U220, and U320 in the figure are the measurement data of each measuring point, and the wetting layer front depth of the curve is calculated using the improved GA model. When the rainfall duration is less than 114 min ($t < 114$ min), the pore water pressure at each measurement point did not change significantly. When $t = 114$ min, the pore water pressure at measurement point U220 began to increase, indicating that the wetting front has reached 20 cm depth at this time. The

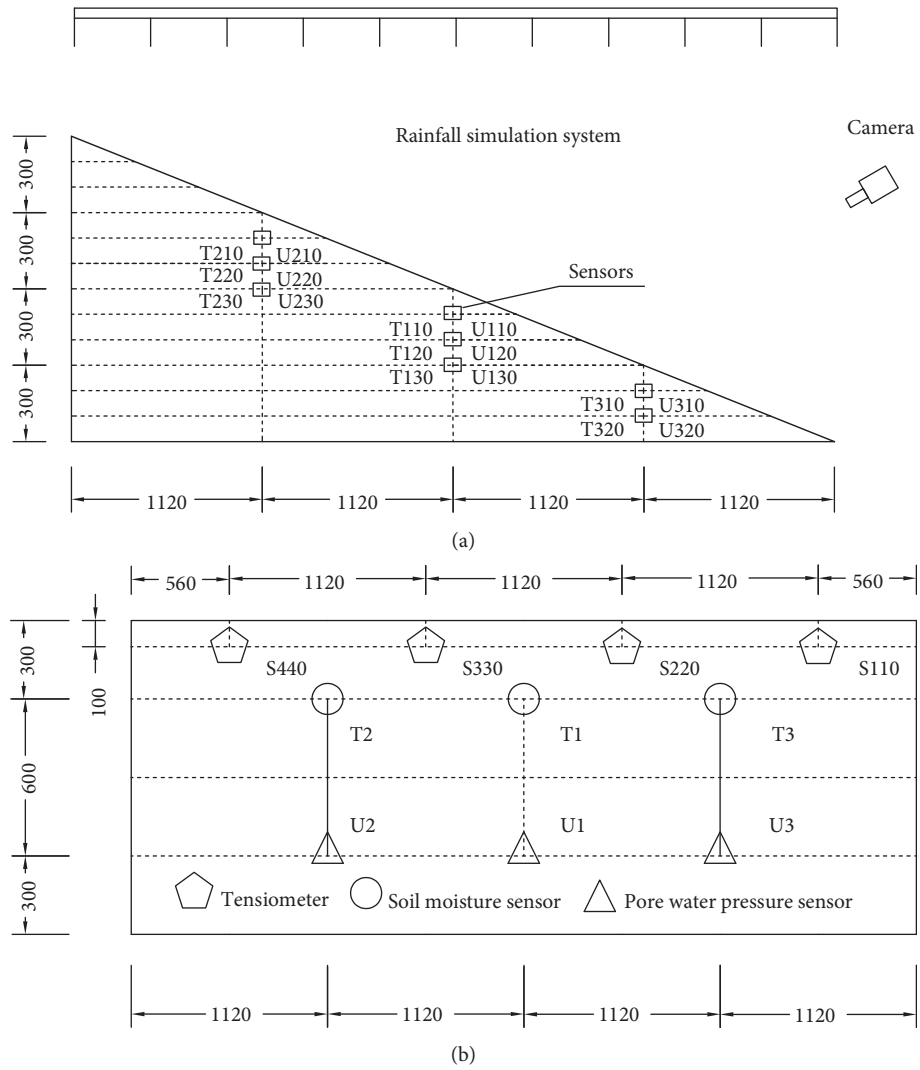

Figure 5: Detection equipment installation location map (distance measured in mm): (a) sensor burial location map; (b) sensor location plan.

Table 1: Properties of tailing soil at 5 cm depth.

Property	Value
Natural moisture content, ω (%)	12.3
Natural density, ρ (g/cm^3)	1.84
Granule density, G_s (g/m^3)	2.71
Saturated permeability coefficient (cm/s)	4.15×10^{-4}
Poisson's ratio, e	0.33
Liquid limit, W_L (%)	26.7
Plastic limit, W_p (%)	16.1
S_f (m)	1.0
S_f' (m)	0.8

pore water pressure at U120 and U320 measurement points only started to increase when $t = 114$ min, mainly because the rainfall intensity at U120 and U320 measurement points was less than 20 mm/h due to the distance from the rainfall point. After the wetting front reached each measurement point, the pore water pressure continued to increase until $t = 182$ min, and the saturated layer reached 20 cm, which further confirmed the obvious stratification phenomenon in the wetting layer. According to the response time of pore water pressure and water content sensor, the average depth ratio of transition layer to wetted layer is 0.43 when the depth of the wetted layer reaches 20 cm, $t = 117$ min, which is basically consistent with the model test results and verifies the correctness of the improved GA model.

4.2. Comparative Analysis of Infiltration Models. To further validate the method proposed in this paper, the GA model, the improved GA model, and Richards' equation [35] were compared with the dynamic change law of wetting front and infiltration rate of unsaturated tailings soil slopes under rainfall conditions. In this paper, Geo-studio is used to establish the numerical model and Seep/W module to solve Richards' equation [36, 37]. The computational model is built with the 2.2 model, and the full mechanics parameters and seepage characteristics parameters are shown in 3.1.

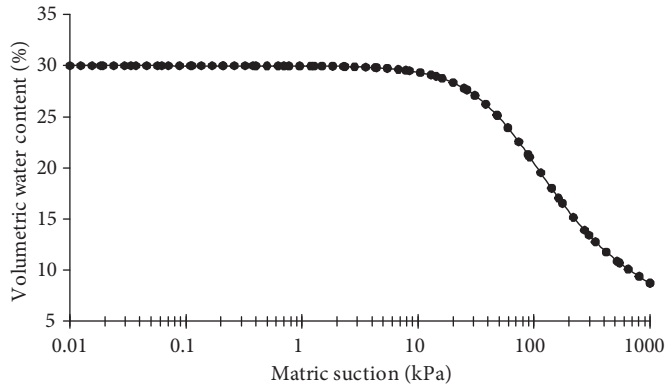

Figure 6: Soil and water characteristic curve.

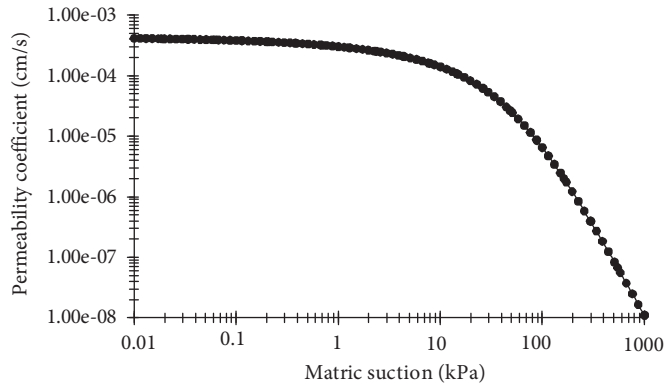

Figure 7: Permeability coefficient curve.

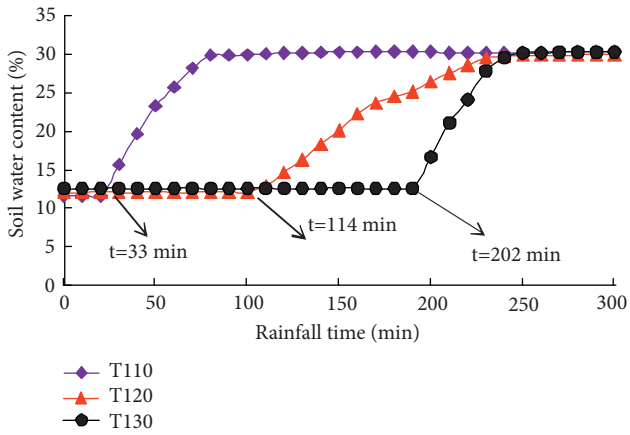

Figure 8: Variation curve of water content with rainfall calendar time.

Richards' equation model is shown in Figure 10, with 591 cells and 645 nodes of the grid. The slope surface of the slope is set as the rainfall boundary, and the bottom and both sides of the slope are set as the impermeable boundary. Monitoring lines of rainfall intensity and infiltration depth are shown in 2.3.

The relationship between wetting front depth and time in the GA model, the improved GA model, and Richards' equation calculation model is shown in Figure 11. It can be seen from Figure 11 that the depths of the wetting fronts of the three models match well at the beginning ($t < 30$ min), and the differences are small. With the increase of rainfall time, the difference of wet front depth of the three models starts to increase. When rainfall time is 152 min, the depth of the wet front obtained by Richards' equation calculation model is about 0.47 m larger than that of the improved GA model. When rainfall time increases to 722 min, the difference increases to 0.60 m, and then the difference basically stabilizes. The difference between the wet front depth calculated by the GA model and that obtained by the improved GA model and Richards' equation calculation model keeps increasing.

Select T110, T120, and T130 positions, according to the time when the wetting front reaches the depth, compare the calculated values of the three models with the measured values of the infiltration test, as shown in Table 2. It can be seen that the calculated values of layered assumption model are in good agreement with the measured data. The improved GA model is only slightly higher than the measured value, with a maximum deviation of about 27 min. However, the GA model deviates from the measured values, and the deviation increases with increasing depth.

Figure 12 shows the rainfall infiltration rate curve of tailings slope with rainfall duration. The infiltration rate of the improved GA model in rainfall infiltration stage I is slower than that of the GA model, and the difference between the two is less than 1 mm/h. After reaching the rainfall

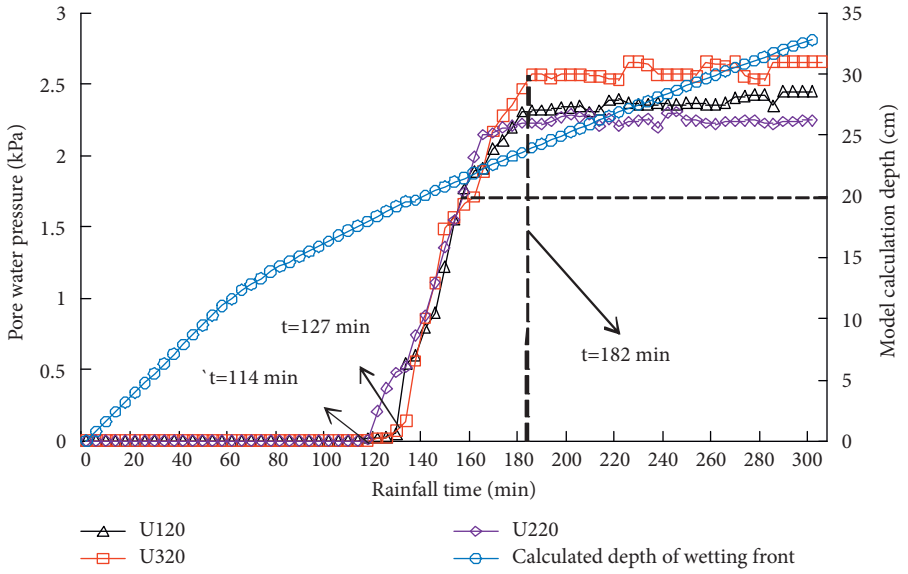

Figure 9: Pore water pressure and calculated depth in different locations at the same depth.

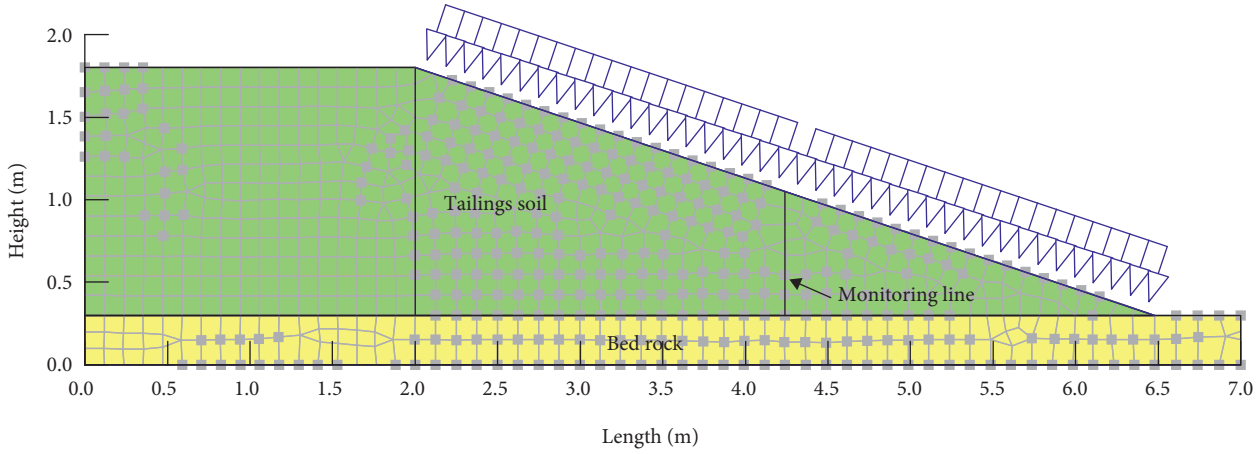

Figure 10: Calculation model.

infiltration stage II, the infiltration rate of the improved GA model gradually exceeds that of the GA model. The gap between the two models reaches the maximum of 4 mm/h at 70 min, then gradually decreases with the continuous infiltration, and remains at 2 mm/h. The rainfall duration for ponding infiltration calculated by the modified GA model and GA model is 30 min and 46 min, respectively. The GA model is 22 min slower than the measured value, while the modified GA model is 6 min slower than the measured value. The infiltration depth calculated by the GA model at the beginning of ponding infiltration is 5.1 cm less than the results of the modified GA model.

The GA model and the improved GA model predict slightly different results compared to Richards' equation. Here the GA model predicts smaller ponding time, smaller vertical infiltration depth in early time and higher infiltration depth in later time, and higher infiltration rates for most of the time. Since the infiltration rate is related to the infiltration coefficient and the hydraulic gradient, the

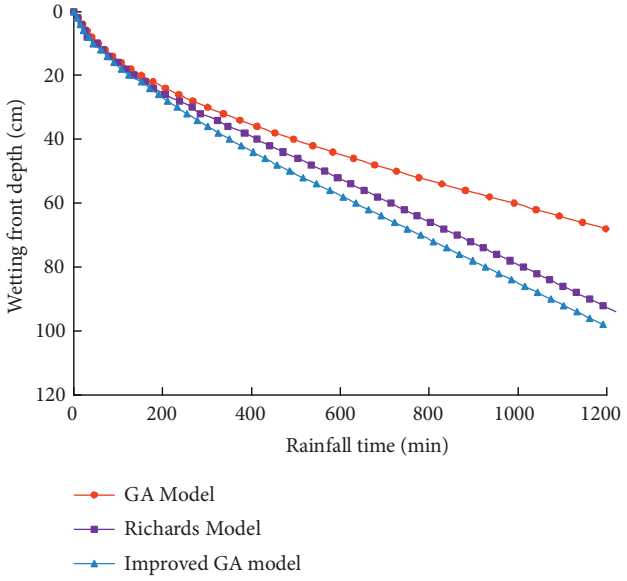

Figure 11: Depth change curve of wetting front.

Table 2: Statistical table of measured data and model calculated parameters.

Type	Arrival time of wetting front/min			Ponding infiltration duration/min	Infiltration depth at the beginning of ponding infiltration/cm
	10 cm	20 cm	30 cm		
GA model	55	153	302	30	7.8
Richards' equation calculation model	52	135	266	—	—
Improved GA model	43	123	229	46	12.9
Measurement	33	114	202	52	—

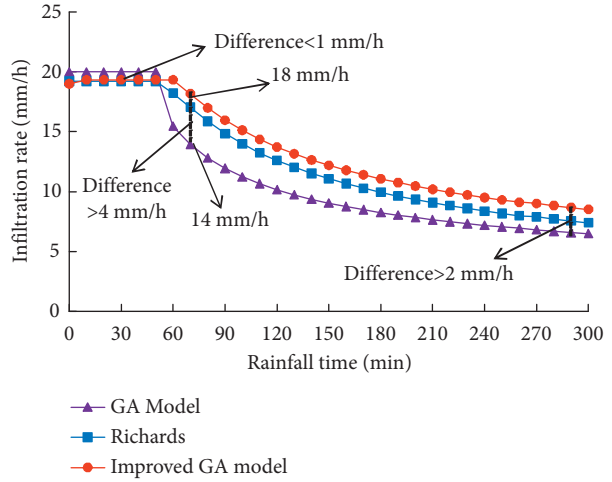

Figure 12: Infiltration rate of the slope with rainfall duration.

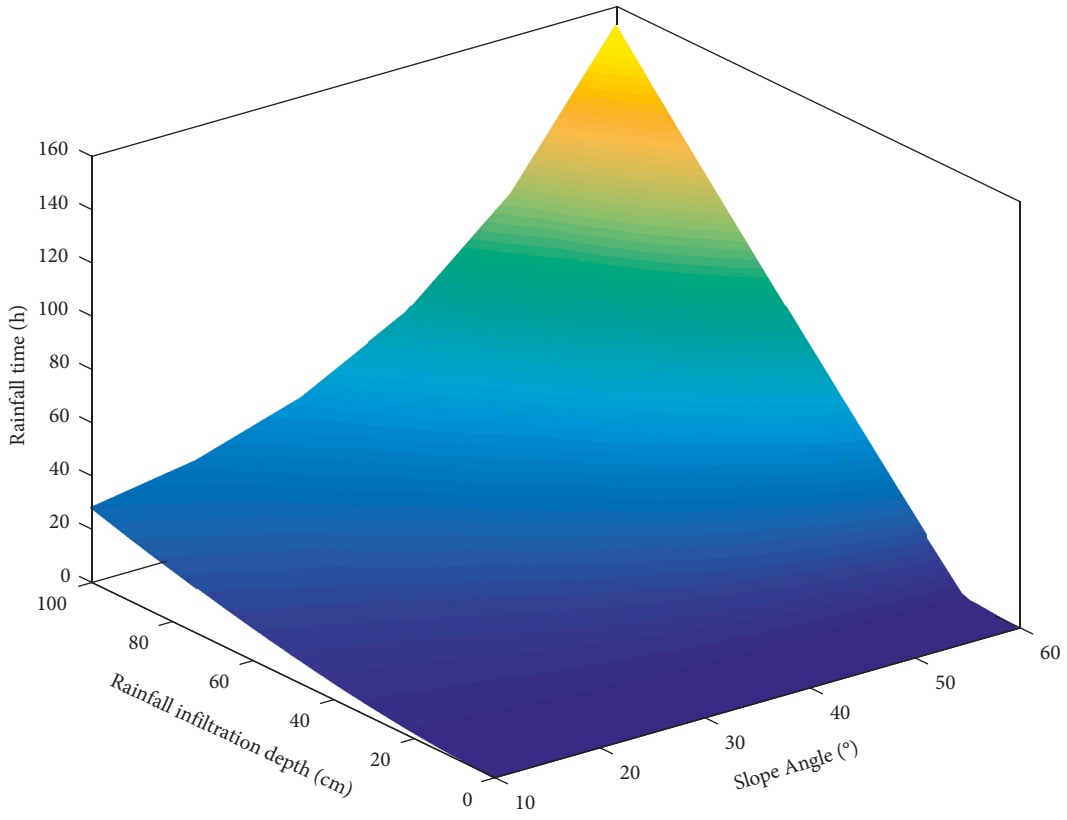

Figure 13: Variation of rainfall infiltration depth in the tailing slope with the changes of rainfall duration and slope angles.

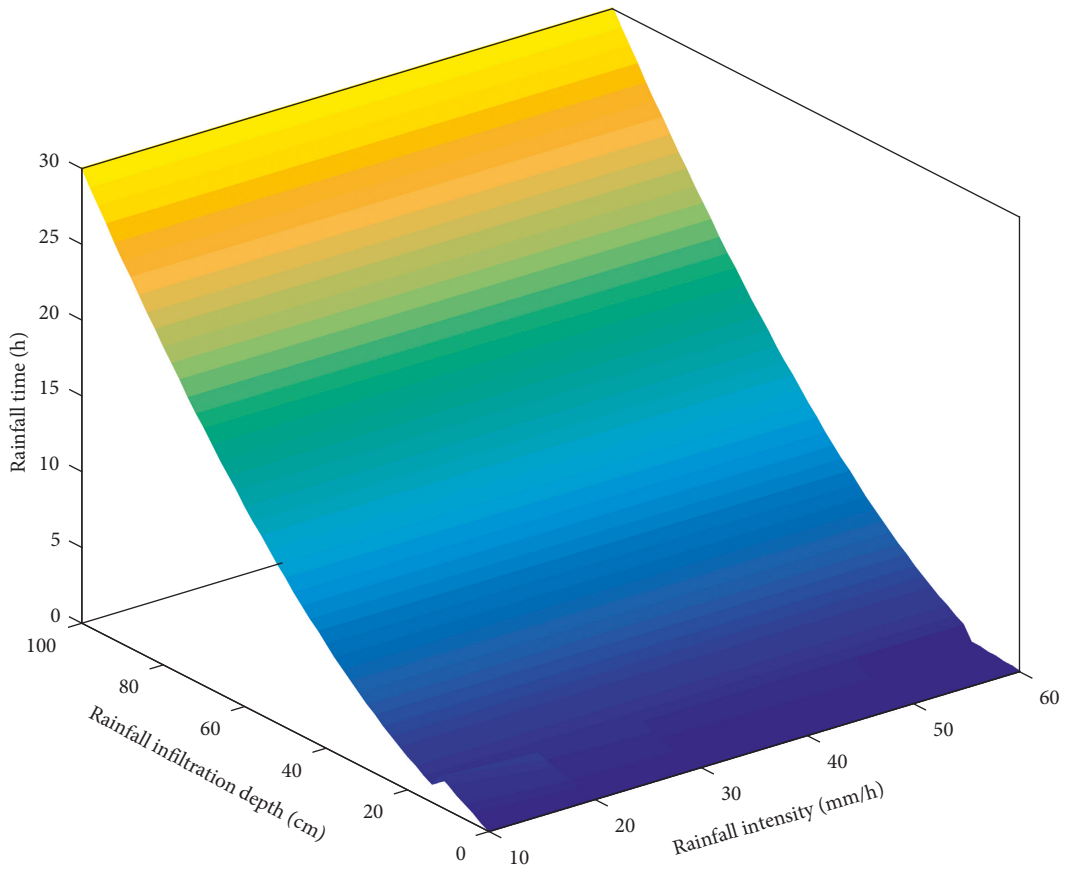

Figure 14: Variation of rainfall infiltration depth in the tailing slope with the changes of rainfall duration and rainfall intensity.

numerical simulation of the improved GA model and Richards' equation calculation model takes into account the effects of the dip angle on the hydraulic gradient and the unsaturated zone on the infiltration coefficient. For the sloping surface case, the improved GA model performs well, capturing both the trend of enhanced infiltration on the slope and the trend of changes in the calculated results of Richards' equation. With the increase of rainfall time, the difference of infiltration rate finally remained basically around 1.52 mm/h. There is a great deviation from the infiltration rate obtained by GA model.

There are two main model differences reasons: (1) The stratification assumption model corrects for the cumulative infiltration of rainfall infiltration processes. (2) The average matrix suction head of the unsaturated layer is regarded as the matrix potential on the saturated layer, and the effects of slope angle and the ratio of the transition layer to the wetted layer are taken into account, thus correcting the conventional GA model.

4.3. Influence Factors of Rainfall Infiltration

4.3.1. Tailings Pond Slope Angle. Figure 13 shows the variation of rainfall infiltration depth in the tailing slope with the changes of rainfall duration and slope angles when the initial water content is 12%, the rainfall intensity is 20 mm/h, and the saturation infiltration coefficient is 4.15×10^{-4} cm/s. The rainfall time required for rainfall to infiltrate to the same depth of the slope body increases with increasing slope angle, and this phenomenon is more significant when the slope angle is greater than 60°. The reason is that when the slope angle exceeds 60°, the gradient of rainfall and infiltration potential energy per unit area of slope surface decreases greatly, which causes more difficulty in the infiltration of rainfall in the soil of the slope.

4.3.2. Rainfall Intensity. When the slope angle is 30°, the initial water content is 12%, the saturation infiltration coefficient is 4.15×10^{-4} cm/s, the variation of rainfall infiltration depth in the tailing slope with the changes of rainfall duration and rainfall intensity is shown in Figure 14. It can be seen that the rainfall ephemeris required for rainfall infiltration to the same depth of the slope decreases with the increase of rainfall intensity, and this phenomenon is more obvious when the rainfall intensity is less than 20 mm/h. From 1.2 above, it can be seen that, in stage I of rainfall infiltration, rainfall intensity affects the amount of rainfall received on the slope unit area, thus affecting the infiltration of slope soil, and the rate of rainfall infiltration is determined by rainfall intensity; however, when rainfall infiltration reaches stage II, it can be seen from Figure 4 that rainfall intensity exceeding 20 mm/h has less influence on rainfall

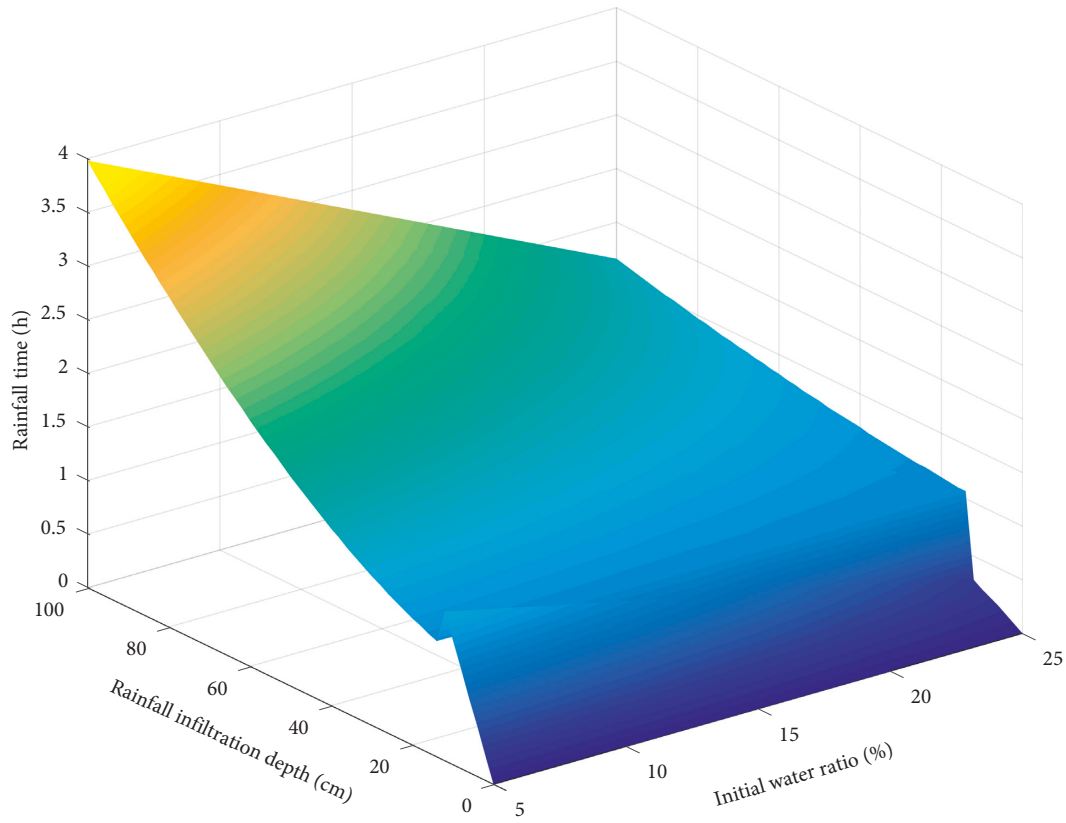

Figure 15: Variation of rainfall infiltration depth in the tailing slope with the changes of rainfall duration and initial water content.

infiltration, which is because the rate of rainfall infiltration in this stage is controlled by the infiltration capacity of slope soil and is not related to rainfall intensity. Therefore, rainfall intensity mainly affects the relationship between infiltration depth and rainfall duration with the slope ponding infiltration time changes.

4.3.3. Initial Water Content. When the slope angle is 30°, the rainfall intensity is 20 mm/h, and the saturation infiltration coefficient is 4.15×10^{-4} cm/s. The variation of rainfall infiltration depth in the tailing slope with the changes of rainfall duration and initial water content is shown in Figure 15. The rainfall duration required for rainfall infiltration to the same depth in the slope decreases gradually with increasing initial water content, and this phenomenon is more obvious at an initial water content of 25%. This is caused by the increase of rainfall infiltration depth in the tailings soil with the increase of initial water content. The effect of initial water content on the depth of infiltration of the model response deepens with time for a constant infiltration time.

4.3.4. Saturation Permeability Coefficient. When the slope angle is 30°, the rainfall intensity is 20 mm/h, and the initial moisture content is 12%, the variation of rainfall infiltration depth in the tailing slope with the changes of rainfall duration and infiltration coefficient is shown in Figure 16. The rainfall duration required for rainfall infiltration at the same depth gradually increases with the decrease of permeability coefficient, which is more obvious when the saturated infiltration coefficient is 2×10^{-4} cm/s. The influence of soil permeability coefficient on rainfall infiltration becomes more significant with the increase of depth. The reason is that the infiltration rate of rainfall is controlled by the infiltration capacity of slope soil in stage II of water infiltration.

4.4. Sensitivity Analysis of Influencing Parameters of Rainfall Infiltration. In this paper, the rainfall infiltration impact parameters are normalized (Table 3) [38, 39] and sensitivity analysis is conducted according to the sensitivity classification [40].

The amplitude of variation of the key model parameters β, q, θ_i, and k_s is uniformly set to 20% [23, 40], and the sensitivity index is calculated as follows:

$$I = \left(\frac{\Delta O}{\Delta F_i}\right)\left(\frac{F_i}{O}\right), \tag{19}$$

where O is the model output; F_i is the parameters that affect the model output results; ΔO is the change value of the model output result; and ΔF_i is the amount of parameter change that affects the model output results.

The results of the sensitivity index calculations for the key parameters affecting the depth of rainfall infiltration are shown in Table 4. The positive and negative signs in the table indicate that the parameter changes are positively or negatively correlated with the model calculated values [40].

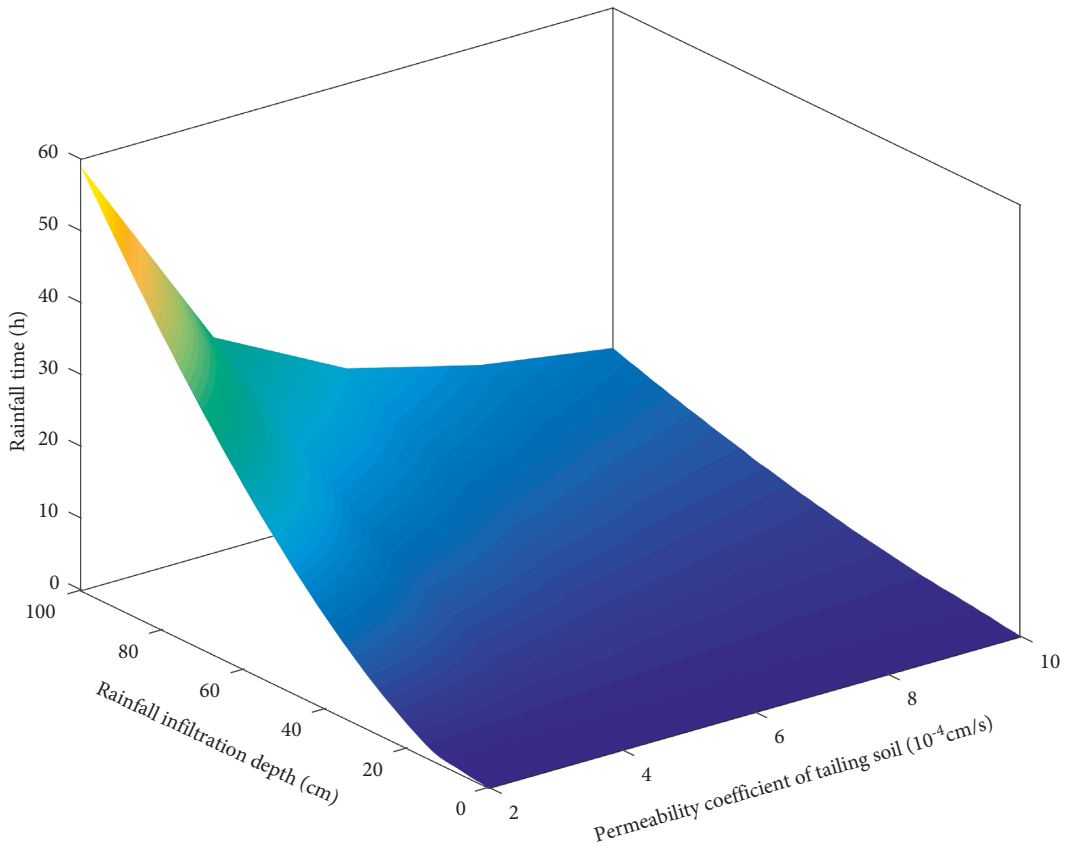

Figure 16: Variation of rainfall infiltration depth in the tailing slope with the changes of rainfall duration and infiltration coefficient.

Table 3: Parameter sensitivity classification.

Classification	Index	Susceptibility
I	$0 \le \lvert I \rvert \le 0.05$	Insensitive
II	$0.05 \le \lvert I \rvert \le 0.2$	Commonly sensitive
III	$0.2 \le \lvert I \rvert \le 1$	Highly sensitive
IV	$\lvert I \rvert \ge 1$	Overwhelming sensitive

Table 4: Sensitivity analysis of rainfall infiltration depth.

Number	Input parameters	Value range	Output objective function (depth of infiltration at different times) corresponding to sensitivity index						Sensitivity level
			h_{30}	h_{60}	h_{90}	h_{120}	h_{180}	h_{240}	
1	β	20	0.17	−1.06	−3.99	−6.13	−7.51	−8.79	IV
		−20	0.17	0.57	4.23	5.42	5.97	5.91	IV
2	q	20	0.32	−0.05	−0.16	−0.26	−0.34	−0.38	III
		−20	−0.04	−0.16	−0.22	−0.26	−0.29	−0.3	III
3	θ_i	20	0.08	0.07	0.23	0.31	0.39	0.42	III
		−20	0.32	−0.05	−0.16	−0.26	−0.34	−0.38	III
4	k_s	20	<0.05	<0.05	0.1	0.09	0.08	0.08	II
		−20	<0.05	−0.11	−0.1	−0.09	−0.08	−0.08	II

From Table 4, it can be seen that the four model parameters ranked by the sensitivity are $\beta \ge \theta_i \ge q \ge k_s$. When the angle of tailings slope increases by 20%, the sensitivity index belongs to grade IV, and the maximum sensitivity index attains 8.79. However, when it goes down by 20%, the sensitivity index belongs to class IV. When the model parameter saturation permeability coefficient is floated up by 20%, its maximum sensitivity coefficient is 0.1. When it goes down by 20%, its maximum sensitivity index is 0.11, and its sensitivity index belongs to class II. At the same time, when

the two model parameters of rainfall intensity and initial water content float up and down by 20%, the sensitivity indices are relatively the same, both of which belong to class III. Therefore, when applying this model for tailings dam slope design and stability evaluation, the parameters β and θ_i should be considered first.

5. Conclusions

The existing infiltration depth prediction model only includes a single factor; thus the GA model is modified to enhance its applicability.

(1) The relationship between wet front depth and rainfall time predicted by the improved GA model is closer to the actual value of the infiltration test than that calculated by the GA model and Richards' equation and has higher accuracy. In the time period of free infiltration, the difference between the wetting front extensions of the three models is small. With the increase of rainfall duration, the infiltration depths obtained from the improved GA model and Richards' equation are consistent with each other. The difference between the two infiltration depths tends to be stable, but the difference with the GA model infiltration depth becomes larger.

(2) At the initial stage of infiltration, the expansion rate of the wetting front of the three models is faster, and the infiltration rates of the improved GA model and Richards' equation are smaller than those of the GA model. After reaching the stage of water infiltration, the transport speed of the wetting front tends to decrease, and the infiltration rates of the three models decrease rapidly. The change of infiltration rate calculated by the improved GA model and Richards' equation tends to be consistent, and the results are larger than those of the GA model. This difference becomes smaller with the continuation of infiltration.

(3) The effect of slope angle, rainfall intensity, initial water content, and saturated permeability coefficient and other parameters on slope rainfall infiltration is analyzed by using the improved GA model. The influence parameters have a critical value, and the influential effect on the infiltration of rainfall on the slope will change abruptly when the critical value is exceeded.

(4) When applying this model to the rainfall infiltration in tailings slopes, the influence of slope angle and initial water content should be focused on to provide the theoretical basis for the construction and stability research of tailings dams in the future.

Data Availability

The data that support the findings of this study are available from the corresponding author upon reasonable request.

Conflicts of Interest

The authors declare that they have no conflicts of interest.

Acknowledgments

The research was supported by the Major Science and Technology Program for Water Pollution Control and Treatment, China (no. 2015ZX07202-012), the Project of Natural Science Foundation of Liaoning Province, China (no. 20180550192), the Liaoning BaiQianWan Talents Program, China (no. [2015]33), the Project of Science and Technology of Liaoning Province, China (no. 2019JH8/10300107 and no. 2020JH2/10300100), the Special Project of Guiding Local Scientific and Technological Development by the Central Government of Liaoning Province (no. 2021JH6/10500015), the Science and Technology Development Plan of Weifang, China (no. 2019GX089), and the Program of Study Abroad for Young Scholar sponsored by Shandong Transport Vocational College, China (no. 201909).

References

[1] K. Stefaniak, M. Wróżyńska, and M. Kroll, "Application of postflotation tailings in hydroengineering structures," *Journal of Ecological Engineering*, vol. 18, no. 1, pp. 113–118, 2017.

[2] N. M. Rana, N. Ghahramani, S. G. Evans, S. McDougall, A. Small, and W. A. Take, "Catastrophic mass flows resulting from tailings impoundment failures," *Engineering Geology*, vol. 292, Article ID 106262, 2021.

[3] G. Cao, W. Wang, G. Yin, and Z. Wei, "Experimental study of shear wave velocity in unsaturated tailings soil with variant grain size distribution," *Construction and Building Materials*, vol. 228, Article ID 116744, 2019.

[4] C. L. Paulina and L. Upmanu, "Tailings dams failures: updated statistical model for discharge volume and runou," *Environments*, vol. 5, no. 2, 2018.

[5] L. M. Albu, A. Enea, M. Iosub, and I. G. Breabăn, "Dam breach size comparison for flood simulations.a hec-ras based GIS approach for Drăcşani Lake, Sitna River, Romania," *Water*, vol. 12, no. 4, 1090 pages, 2020.

[6] L. Z. Wu, J. S. Huang, W. Fan, and X. Li, "Hydro-mechanical coupling in unsaturated soils covering a non-deformable structure," *Computers and Geotechnics*, vol. 117, Article ID 103287, 2019.

[7] Y. Jeong and K. Kim, "A case study:Determination of the optimal tailings beach distance as a guideline for safe water management in an upstream TSF," *Mining, Metallurgy & Exploration*, vol. 37, no. 1, pp. 141–151, 2020.

[8] D. Łydżba, A. Różański, M J. Sobótka et al., "Safety analysis of the Żelazny most tailings pond: qualitative evaluation of the preventive measures effectiveness," *Studia Geotechnica et Mechanica*, vol. 43, no. 2, pp. 181–194, 2021.

[9] G. D. Liu, Z. J. Zhou, S. Q. Xu, W. J. Mi, and J. Pitthaya, "Experimental assessments of treating effect on retaining walls for loess slopes under long-term rainfall," *Advances in Civil Engineering*, vol. 202123 pages, Article ID 5542727, 2021.

[10] H. Green and G. A. Ampt, "Studies on soil physics: Part II — the permeability of an ideal soil to air and water," *The Journal of Agricultural Science*, vol. 5, no. 1, pp. 1–26, 1912.

[11] R. V. Kale, B. Sahoo, and S H. Bhabagrahi, "Green-ampt infiltration models for varied field conditions:A revisit," *Water Resources Management*, vol. 25, no. 14, pp. 3505–3536, Article ID 3505, 2011.

[12] L. Chen and M. H. Young, "Green-Ampt infiltration model for sloping surfaces," *Water Resources Research*, vol. 42, no. 7, Article ID 7420, 2006.

[13] J. Mohammadzadeh-Habili and M. Heidarpour, "Application of the Green-Ampt model for infiltration into layered soils," *Journal of Hydrology*, vol. 527, pp. 824–832, 2015.

[14] P. Deng and J. Zhu, "Analysis of effective Green-Ampt hydraulic parameters for vertically layered soils," *Journal of Hydrology*, vol. 538, pp. 705–712, 2016.

[15] W. M. Yao, C. D. Li, H. B. Zhan, and J. Zeng, "Time-dependent slope stability during intense rainfall with stratified soil water content," *Bulletin of Engineering Geology and the Environment*, vol. 78, no. 7, pp. 4805–4819, 2019.

[16] R. Ojha, C. Corradini, R. Morbidelli, R. Govindaraju, M. Govindaraju, and K. Levent, "Effective saturated hydraulic conductivity for representing field-scale infiltration and surface soil moisture in heterogeneous unsaturated soils subjected to rainfall events," *Water*, vol. 9, no. 2, 134 pages, Article ID 9020134, 2017.

[17] Y. Wang, Y. J. Zhang, M. F. Li, Y. Qi, and T. H. Ma, "A numerical investigation of the deformation mechanism of a large metro station foundation pit under the influence of hydromechanical processes," *Geofluids*, vol. 202116 pages, Article ID 5536137, 2021.

[18] Z. H. Guo, W. B. Jian, Q. L. Liu, and W. Nie, "Rainfall infiltration analysis and infiltration model of slope based on in-situ tests," *Rock and Soil Mechanics*, vol. 42, pp. 1635–1647, 2021.

[19] L. Sanghyun, L. Maria, and A. R. Chu, "Schmidt, "effective green-ampt parameters for two-layered soils," *Journal of Hydrologic Engineering*, vol. 25, no. 4, 2020.

[20] J. Fernández-Pato, J. L. Gracia, and P. García-Navarro, "A fractional-order infiltration model to improve the simulation of rainfall/runoff in combination with a 2D shallow water model," *Journal of Hydroinformatics*, vol. 20, no. 4, pp. 898–916, 2018.

[21] S. E. Cho, "Prediction of shallow landslide by surficial stability analysis considering rainfall infiltration," *Engineering Geology*, vol. 231, no. 14, pp. 126–138, 2017.

[22] Y. B. Pan, W. Z. Jian, and L. J. Li, "A study on the rainfall infiltration of granite residual soil slope with an improved Green-Ampt model," *Rock and Soil Mechanics*, vol. 41, pp. 2685–2692, 2020.

[23] X. Wen, Z. P. Hu, X. Zhang, S. B. Chai, and X. B. Lv, "Modified infiltration model for saturated-unsaturated loess based on Green-Ampt model and its parametric study," *Rock and Soil Mechanics*, vol. 41, no. 6, pp. 1991–2000, 2020.

[24] Z. Y. Peng, J. S. Huang, and J. W. Wu, "Modification of Green-Ampt model based on the stratification hypothesis," *Advances in Water Science*, vol. 23, no. 1, pp. 59–66, 2012.

[25] G. Q. Cai, M. Z. Li, B. Han, K. Di, Q. Q. Liu, and J. Li, "Numerical analysis of unsaturated soil slopes under rainfall infiltration based on the modified glasgow coupled model," *Advances in Civil Engineering*, vol. 202013 pages, Article ID 8865179, 2020.

[26] Z. Z. Liu, Z. X. Yan, Z. H. Qiu, X. G. Wang, and J. W. Li, "Stability analysis of an unsaturated soil slope considering rainfall infiltration based on the Green-Ampt model," *Journal of Mountain Science*, vol. 17, no. 10, pp. 2577–2590, 2020.

[27] H. Y. Zhu and X. H. Duan, "Progress of foreign research on Green-Ampt infiltration model," *China Rural Water Conservancy and Hydropower*, vol. 10, no. 6, pp. 12–22, 2017.

[28] R. G. Mein and C. L. Larson, "Modeling infiltration during a steady rain," *Water Resources Research*, vol. 9, no. 2, pp. 384–394, 1973.

[29] H. Bouwer, "Rapid field measurement of air entry value and hydraulic conductivity of soil as significant parameters in flow system analysis," *Water Resources Research*, vol. 2, no. 4, pp. 729–738, 1966.

[30] Z. Jovanov, A. Strašeski, B. J. Papić, I. Ljubenkov, and B. Susinov, "Impact of unsaturated strength-deformability properties on stress-deformation condition and stability of tailing dams," *Ce/Papers*, vol. 2, no. 2-3, pp. 677–682, 2018.

[31] E. A. Colman and G. B. Bodman, "Moisture and energy conditions during downward entry of water into moist and layered soils," *Soil Science Society of America Journal*, vol. 9, no. C, pp. 3–11, 1945.

[32] J. M. Habili and M. Heidarpour, "Application into layered of the Green-Ampt model for infiltration into layered soils," *Journal of Hydrology*, vol. 527, pp. 824–832, 2015.

[33] W. Y. Wang, Z. R. Wang, Q. J. Wang, and J. F. Zhang, "Improvement and validation of Green-Ampt infiltration model in loess," *Journal of Water Resources*, vol. 05, pp. 30–34, 2003.

[34] D. Zhang, Y. Huang, and J. L. He, "Study on Green-Ampt model of soil moisture changes with depth in wet area," *Journal of Irrigation and Drainage*, vol. 35, no. 12, pp. 60–66, 2016.

[35] L. L. Zhang, D. G. Fredlund, L. M. Zhang, and W. H. Tang, "Numerical study of soil conditions under which matric suction can be maintained," *Canadian Geotechnical Journal*, vol. 41, no. 4, pp. 569–582, 2004.

[36] J. Zhang, T. Lv, J. F. Xue, and W. T. Cheng, "A modified Green-Ampt model applicable to slope rainfall infiltration analysis," *Geotechnics*, vol. 37, no. 09, pp. 2451–2457, 2016.

[37] T. Lv, J. Zhang, J. F. Xue, H. W. Huang, and Y. T. Yu, "Study on the method of taking the infiltration coefficient of Green-Ampt model," *Geotechnics*, vol. 36, no. 1, pp. 341–345, 2015.

[38] L. M. Tian, C. L. Qu, and J. H. Zhang, "Analysis of particle deposition law and dam seepage field of upstream tailings pond," *Metal Mine*, vol. 5, no. 1, pp. 60–64, 2017.

[39] A. Wang and L. Tang, "Analysis of comprehensive sensitivity coefficient of hydrological model parameters," *Hydro*, vol. 43, no. 16, pp. 18–64, 2017.

[40] M. M. Liu, L. Duan, C. Zhang, H. Song, T. T. Lv, and S. L. Huo, "Sensitivity analysis of hydraulic parameters of one-dimensional water transport model," *China rural water resources and hydropower*, vol. 5, no. 41, pp. 131–135, 2019.